

R.L. (2)

# NAVAL POSTGRADUATE SCHOOL

## Monterey, California

AD-A269 064



THESIS

DTIC  
ELECTE  
SEP 09 1993  
S E D

Developmental Testing of a Prototype  
All-Reflection Michelson Interferometer

by

Allan David Risley, Jr.

June, 1993

Thesis Advisor:

David D. Cleary

Approved for public release; distribution is unlimited.

93-20913



REPORT DOCUMENTATION PAGE			Form Approved OMB No. 0704-0188	
<small>Public reporting burden for this collection of information is estimated to average 1 hour per response, including the time for reviewing instructions, searching existing data sources, gathering and maintaining the data needed, and completing and reviewing the collection of information. Send comments regarding this burden estimate or any other aspect of this collection of information, including suggestions for reducing this burden, to Washington Headquarters Services, Directorate for Information Operations and Reports, 1215 Jefferson Davis Highway, Suite 1204, Arlington, VA 22202-4302 and to the Office of Management and Budget, Paperwork Reduction Project (0704-0188), Washington, DC 20503.</small>				
1. AGENCY USE ONLY (Leave blank)	2. REPORT DATE June, 1993	3. REPORT TYPE AND DATES COVERED Master's Thesis		
4. TITLE AND SUBTITLE Developmental Testing of a Prototype All-Reflection Michelson Interferometer		5. FUNDING NUMBERS		
6. AUTHOR(S)  Allan David Risley, Jr.				
7. PERFORMING ORGANIZATION NAME(S) AND ADDRESS(ES) Naval Postgraduate School Monterey, CA 93943-5000		8. PERFORMING ORGANIZATION REPORT NUMBER		
9. SPONSORING/MONITORING AGENCY NAME(S) AND ADDRESS(ES) Naval Postgraduate School Monterey, CA 93943-5000		10. SPONSORING/MONITORING AGENCY REPORT NUMBER		
11. SUPPLEMENTARY NOTES The views expressed in this thesis are those of the author and do not reflect the official policy or position of the Department of Defense or the U.S. Government.				
12a. DISTRIBUTION/AVAILABILITY STATEMENT  Approved for public release; distribution is unlimited.		12b. DISTRIBUTION CODE		
13. ABSTRACT (Maximum 200 words) A prototype all-reflective Michelson interferometer is tested using visible laser, sodium, and mercury light sources. The design uses an off-axis parabolic mirror for collimation, a plane diffraction grating and two plane mirrors to divide and recombine incident light. Interference fringes were seen using the laser light source, but instrument performance with other sources was unreliable as a result of difficulties in constructing the instrument with enough mechanical precision. A method of using a full-size template to position the instrument's optical elements was discovered, and the efficacy of an image intensifier/photodiode array combination for use as a detector was verified. The feasibility of the interferometer design was verified by the observation of interference fringes using mercury 5461 A light. A practical instrument would be compact, light weight, and require no moving parts.				
14. SUBJECT TERMS Spectroscopy, Interferometer.		15. NUMBER OF PAGES 51		
		16. PRICE CODE		
17. SECURITY CLASSIFICATION OF REPORT UNCLASSIFIED	18. SECURITY CLASSIFICATION OF THIS PAGE UNCLASSIFIED	19. SECURITY CLASSIFICATION OF ABSTRACT UNCLASSIFIED	20. LIMITATION OF ABSTRACT SAR	

Approved for public release; distribution is unlimited.

**Developmental Testing of a Prototype  
All-Reflection Michelson Interferometer**

by

Allan David Risley, Jr.  
Lieutenant, United States Navy  
B.S., The Ohio State University, 1985

Submitted in partial fulfillment  
of the requirements for the degree of

**MASTER OF SCIENCE IN PHYSICS**

from the

**NAVAL POSTGRADUATE SCHOOL**  
June 1993

Author:

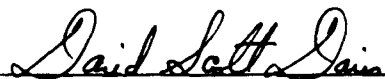


Allan David Risley Jr.

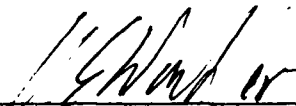
Approved by:



David D. Cleary, Thesis Advisor



D. Scott Davis, Second Reader



Karlheinz E. Woehler, Chairman, Department of Physics

## ABSTRACT

A prototype all-reflective Michelson interferometer is tested using visible laser, sodium, and mercury light sources. The design uses an off-axis parabolic mirror for collimation, a plane diffraction grating and two plane mirrors to divide and recombine incident light. Interference fringes were seen using the laser light source, but instrument performance with other sources was unreliable as a result of difficulties in constructing the instrument with enough mechanical precision. A method of using a full-size template to position the instrument's optical elements was discovered, and the efficacy of an image intensifier/photodiode array combination for use as a detector was verified. The feasibility of the interferometer design was verified by the observation of interference fringes using mercury 5461 Å light. A practical instrument would be compact, light weight, and require no moving parts.

Accession For	
NTIS	CRA&I <input checked="checked" type="checkbox"/>
DTIC	TAB <input type="checkbox"/>
Unannounced	<input type="checkbox"/>
Justification	
By	
Distribution/	
Availability Codes	
Dist	Avail and/or Special
A-1	

## TABLE OF CONTENTS

<b>I.</b>	<b>INTRODUCTION.....</b>	<b>1</b>
<b>A.</b>	<b>THESIS OBJECTIVE.....</b>	<b>2</b>
<b>B.</b>	<b>THESIS OUTLINE.....</b>	<b>2</b>
<b>II.</b>	<b>BACKGROUND.....</b>	<b>3</b>
<b>A.</b>	<b>THE EARTH'S ATMOSPHERE.....</b>	<b>3</b>
1.	Temperature and Composition Profiles.....	3
2.	The Ionosphere .....	4
3.	Ionospheric Observations.....	7
<b>B.</b>	<b>SPECTROSCOPY .....</b>	<b>8</b>
1.	Atomic and Molecular Emissions.....	8
2.	Line-Broadening Mechanisms .....	10
<b>III.</b>	<b>THEORY .....</b>	<b>12</b>
<b>A.</b>	<b>INTERFERENCE.....</b>	<b>12</b>
<b>B.</b>	<b>DIFFRACTION .....</b>	<b>16</b>
<b>C.</b>	<b>THE ALL-REFLECTION MICHELSON INTERFEROMETER..</b>	<b>19</b>
<b>IV.</b>	<b>EXPERIMENT .....</b>	<b>25</b>
<b>A.</b>	<b>CONSTRUCTION OF ALL-REFLECTIVE INSTRUMENT .....</b>	<b>25</b>
<b>B.</b>	<b>TESTING WITH SODIUM VAPOR LAMP SOURCE .....</b>	<b>29</b>
<b>C.</b>	<b>TESTING WITH MERCURY VAPOR LAMP SOURCE .....</b>	<b>30</b>
<b>D.</b>	<b>TESTING WITH ULTRAVIOLET SOURCE.....</b>	<b>33</b>
<b>V.</b>	<b>RESULTS AND RECOMMENDATIONS .....</b>	<b>39</b>
<b>A.</b>	<b>RESULTS OF EXPERIMENTS .....</b>	<b>39</b>

<b>B. RECOMMENDATIONS FOR FURTHER STUDY .....</b>	<b>40</b>
<b>LIST OF REFERENCES.....</b>	<b>41</b>
<b>INITIAL DISTRIBUTION LIST .....</b>	<b>43</b>

## I. INTRODUCTION

A knowledge of the composition and chemistry of the Earth's atmosphere is invaluable in many fields of activity, from the operation of space vehicles to predicting the weather. Two applications of this knowledge directly relevant to the military are high-frequency radio communications and over-the-horizon radar. Exploiting the electromagnetic properties of the ionosphere requires measurement of the electron density profile, which varies with altitude, time of day, location, season, and the level of solar activity. Currently, this measurement is made with ground-based ionosondes, which provide an accurate map of the electron density above the site but tell little about the ionosphere outside the local area. In order for the ionosphere to be of tactical use, a method of sensing its properties in real time over wide areas must be found.

One potential means of inferring electron density is by studying the atmospheric airglow. Satellite-borne spectrographic equipment could provide information about the entire atmosphere in near real time. The Naval Postgraduate School (NPS) has developed such an instrument, the Middle Ultraviolet Spectrograph (MUSTANG). MUSTANG observes emissions in the range 1800 Å to 3400 Å, with a resolution of approximately 10 Å (Chase, 1992). It was launched aboard NASA sounding rockets in 1990 and 1992 (Walden, 1991; Clayton, 1990), and an improved version is scheduled to be included in a satellite being prepared for launch in 1995 (Atkinson, 1993).

During MUSTANG development, it became evident that an instrument providing higher wavelength resolution through interferometric means would be valuable. Since the emissions of interest lie in the ultraviolet range of the electromagnetic spectrum, such an instrument would need to be constructed using all-reflective optical elements. Nichols

(1990) designed and tested an instrument using plane mirrors and a spherical diffraction grating (Nichols, 1990). Wallace (1992) found that a similar instrument based on a plane diffraction grating would be more suitable because it produces linear interference fringes which are more amenable to analysis using Fourier transforms. He designed and built a prototype instrument using a He-Ne laser as the light source and a 10 cm focal length convex lens for collimation (Wallace, 1992). This thesis is a continuation of that work.

#### **A. THESIS OBJECTIVE**

The objective of this thesis is to perform developmental testing of the instrument designed by Wallace, first replicating his results using an instrument made up solely of reflective optical elements, and then testing the prototype using sources with shorter wavelengths and smaller degrees of spatial coherence. The ultimate goal is to demonstrate the feasibility of the all-reflective Michelson interferometer for studying ultraviolet emissions of the type expected to be encountered in the ionosphere so that development of a practical instrument for space flight can begin.

#### **B. THESIS OUTLINE**

This thesis is divided into five sections. Section II gives background information on the composition of the atmosphere and the dynamic processes that produce the emissions to be studied. Section III provides an overview of the theory describing the physical phenomena being exploited in the interferometer design. Section IV describes the experiments conducted in the course of testing the prototype instrument, and Section V presents the results of the experiments and provides recommendations for further research.



## **II. BACKGROUND**

In this section, general background about the atmosphere of the Earth and the physical processes which make the development of a high-resolution ultraviolet interferometer desirable are given.

### **A. THE EARTH'S ATMOSPHERE**

#### **1. Temperature and composition profiles**

The Earth's atmosphere is described by a series of stacked horizontal layers in which some parameter of interest is constant, or follows some predictable trend. Two common parameters used to describe the atmospheric layers are their chemical composition and the temperature profile versus altitude. The first system discussed here is the classification of the atmosphere by temperature profile.

The lowest 10 km of atmosphere is called the troposphere, and it is distinguished by a decrease in temperature with increasing altitude, from approximately 300K at the surface to around 220K at the top of the layer. The clouds, winds, and pressure variations which make up the weather we observe on the surface are contained mostly in this layer, which is characterized by convective mixing.

The next layer of the atmosphere is called the stratosphere. This is a relatively warm layer due to the absorption of solar radiation by ozone. The temperature reaches a local maximum at the stratopause, at about 45 km, and then falls through the mesosphere, reaching a minimum of approximately 180K at an altitude near 85 km.

Above 85 km, the region known as the thermosphere begins. This part of the atmosphere is characterized by a rapid increase in temperature with altitude up to a level

between 200 km and 500 km, where the temperature reaches an equilibrium between 700K and 2000K, depending on the level of solar activity.

In classifying the atmospheric layers by composition, the lowest 80 km is called the homosphere. In this region, the atmosphere is more-or-less chemically homogeneous. The mixture is mainly comprised of nitrogen, oxygen, and argon, which make up over 99 percent of the atmosphere. The remainder consists of helium, hydrogen, carbon dioxide, and traces of other species. In the homosphere the primary transport mechanism is eddy diffusion, a turbulent mixing which brings about the homogeneous mixture of gases. The overall density of atmospheric constituents falls off exponentially in proportion to a quantity known as scale height, which is based upon the average molecular weight of the molecules making up the atmosphere.

The next 20 km is a transition region called the turbopause. Above 100 km, very little vertical mixing occurs, and the molecules tend to separate due to differences in molecular weight. The density of each of the different species decreases with altitude according to its own scale height. This region is called the heterosphere. At extremely high altitudes, the overall density of particles is so low that collisions are rare, and some high-energy particles may even be able to escape from the Earth's gravitational attraction. This region is called the exosphere. The regions of the atmosphere are depicted in Figure 1.

## **2. The Ionosphere**

The lowest part of the heterosphere, from approximately 50 km to 1000 km in altitude, is called the ionosphere. In this region, the relative lack of vertical mixing combined with an increasing flux of solar photons result in the formation of a partially ionized plasma. Although the atmosphere is electrically neutral as a whole, in this region there exist long-lived positive ions and free electrons. Due to the large difference in

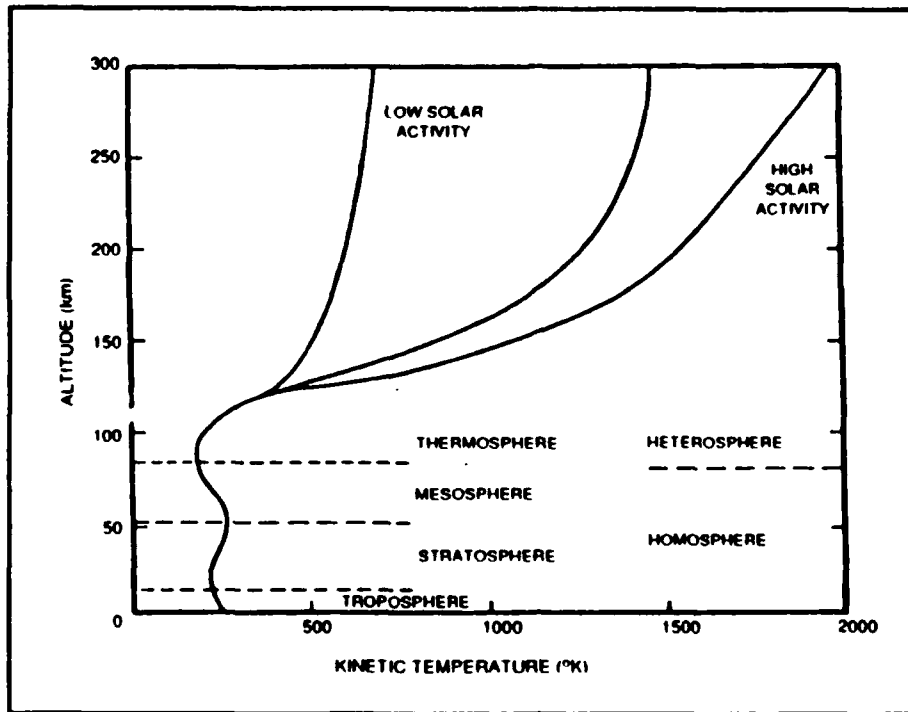


Figure 1 Atmospheric Layers  
(Tascione, 1988)

mass between a molecule and an electron, the electrons are much more mobile. The free electrons interact with electromagnetic waves propagating through this part of the atmosphere, and it is this property which makes the ionosphere interesting from a military point of view. By measuring the electron density, the electrical properties of the ionosphere can be inferred, and possibly exploited tactically.

The main source of ionization in the atmosphere is photoionization, where an incident photon from the sun impacts a neutral atom or molecule forming a positive ion and a free electron. This reaction is depicted below with a general molecule M:



Different molecules absorb at different wavelengths, and the flux of photons at a particular wavelength varies with altitude. High-energy, short wavelength photons penetrate farther into the atmosphere than longer wavelength photons. In the heterosphere, the relative densities of different target molecules also vary with altitude. These effects combine to divide the ionosphere into four layers (D,E,F1, and F2) based upon the relative maxima in the electron density profile. These layers vary with time of day, geographic location, atmospheric composition, and the level of solar activity.

The D layer lies between 50 km and 90 km altitude, and is formed primarily by the ionization of nitric oxide by the solar Lyman- $\alpha$  emission at a wavelength of 1216 Å. This layer disappears rapidly at night because the high density leads to a high loss rate due to recombination of electrons and ions. In addition, the ionization is almost solely a result of the flux of solar photons, which disappears at night.

The E layer lies generally from 90 km to 130 km. The electron density in this region is due mostly to the ionization of molecular oxygen by ultraviolet light and soft X-rays from the sun. For the same reasons as in the D region, the E layer also disappears at night.

The F1 layer is due mainly to the ionization of molecular oxygen by ultraviolet light, and occurs between 140 km and 200 km. The F2 layer lies above 200 km, and results from the presence of  $O^+$ . It is in the F2 region where the electron density reaches its maximum level, around  $10^6$  electrons/cm<sup>3</sup>. The F2 layer can persist at night because the density of particles is so low that collisions leading to recombination of electrons and ions are rare. A plot of typical electron densities versus altitude is given in Figure 2.

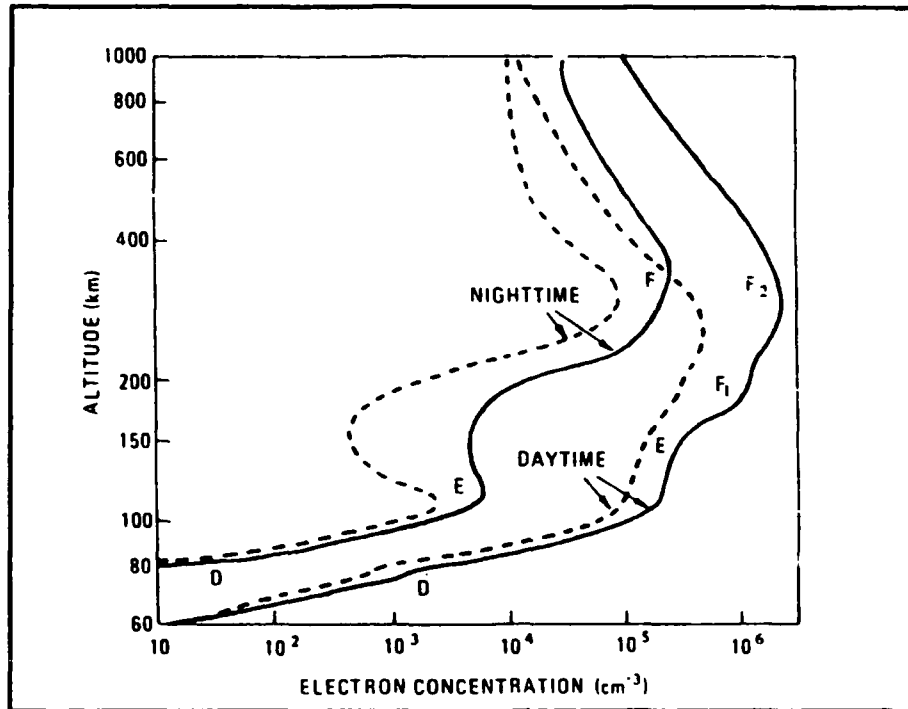


Figure 2 Layers of the Ionosphere  
(Tascione, 1988)

The ionosphere affects electromagnetic radiation by reflecting waves whose frequency is below a "plasma frequency" which depends on the electron density. This is exploited in applications such as long-range communications and over-the-horizon radar.

### 3. Ionospheric Observations

The ionosphere is observed by many means. Using electromagnetic waves of known frequency, ionosondes measure the time between emission and return after reflection from the free electrons in the ionosphere. By varying the frequency of the radiation emitted, this time difference can be used to derive the overhead electron density profile. Spectrographic equipment carried on rockets and satellites measures light emitted by the molecules and ions present in the atmosphere, and use that data to infer information

about the ionosphere. The interferometer being tested in this thesis is designed to provide data for high-resolution analysis of ultraviolet emissions. This will make it possible to understand the composition and photochemistry of the ionosphere in great detail (Cleary et al, 1992). For example, detailed analysis of the atomic oxygen emission at 1304 Å will yield an accurate estimate of the oxygen density.

## **B. SPECTROSCOPY**

### **1. Atomic and Molecular Emissions**

According to Bohr's quantum theory, the allowed orbits of electrons give rise to a series of energy levels for all atoms and molecules. When an electron undergoes a transition from one energy level to a higher energy level, a photon of light is absorbed. If the transition is to a lower energy level, a photon is emitted. The photon has a frequency equal to the difference in energy between the two levels divided by Planck's constant,  $h$ . The system of energy levels gives each type of atom or molecule a distinctive set of characteristic emissions, or spectrum.

Diatomic molecules possess a similar set of electronic energy levels. Superimposed on these levels are sub-levels brought about by the additional degrees of freedom present in the two-atom system. The nuclei of a diatomic molecule repel one another, but the effect of the shared electrons keeps them in an equilibrium condition about which vibration can occur. Additionally, the whole molecule can rotate about an axis through its center of mass, creating another set of energy levels. When transitions between levels occur, photons of light are again emitted or absorbed. A generalized depiction of the system of molecular energy levels is provided in Figure 3.

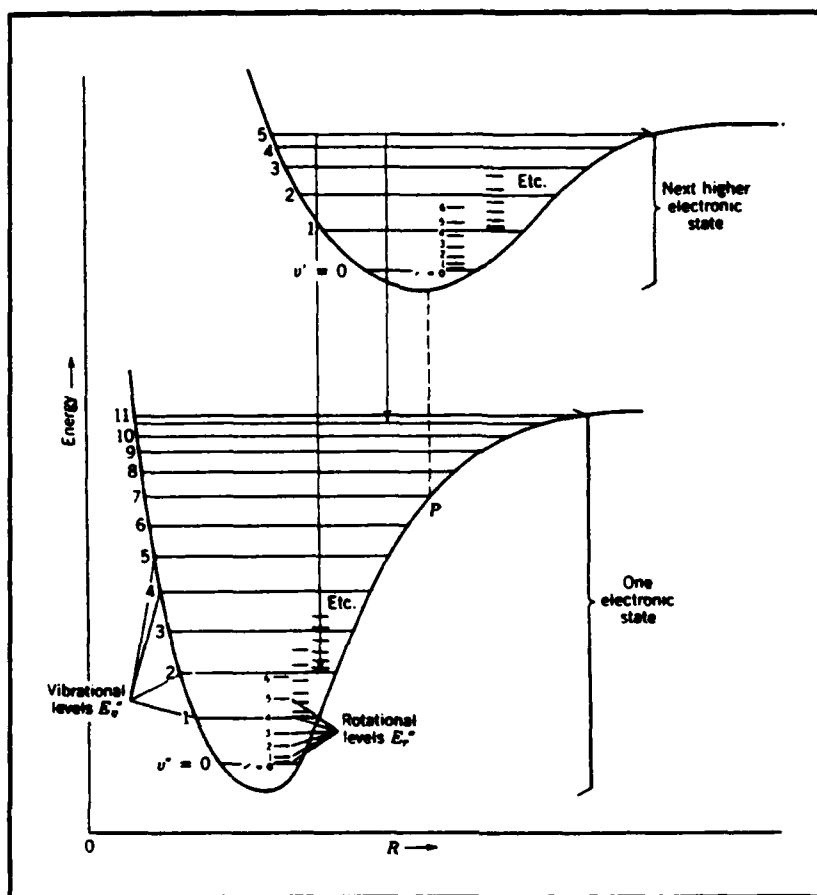


Figure 3 Molecular Energy Levels  
(Eisberg and Resnick, 1985)

An electron which is in a particular vibrational and rotational sub-level of an excited electronic energy state can jump to one of a number of sub-levels of a lower electronic state or the same electronic state, emitting a photon as a result. The relative probabilities of different transitions can be calculated using perturbation theory, a branch of quantum mechanics. This calculation leads to the determination of certain "allowed" and "forbidden" transitions. When the large number of excited molecules in the atmosphere is considered, photons with frequencies corresponding to the full set of allowed transitions between vibration/rotation states of the two electronic energy levels

will be present. This results in a series of closely spaced lines in the emission spectrum of the molecule. These sets of lines are called emission bands. Spectrographic and interferometric instruments can be used to study the band structure of molecular spectra, leading to knowledge of the molecule's density and activity in the atmosphere.

## 2. Line-Broadening Mechanisms

The emissions from molecules and atoms are not monochromatic. Rather, they are a narrow distribution of different wavelengths. The distributions have a finite width which depends on a variety of factors. One way spectral lines are broadened is by natural or lifetime broadening. The width of a spectral line is inversely proportional to the lifetime of the upper state of the transition. A long-lived upper state has a narrow emission line, while a short-lived upper state has a broad emission line. This is a result of Heisenberg's uncertainty principle, which says that the energy of a state and its lifetime can not both be known with infinite precision. The uncertainty in the exact value of the energy leads to a narrow band of wavelengths in the spectrum centered about the wavelength which would result if the energy were known exactly (Dirac, 1958).

Another broadening mechanism is pressure broadening, in which collisions between molecules introduce a similar uncertainty into the magnitude of the energy transition causing the emission. At high altitudes, collisions are rare, so the effect of this mechanism on the width of spectral lines is minimal.

The dominant cause of spectral line broadening in the terrestrial atmosphere is Doppler broadening. Since the molecules are moving as they emit radiation, the frequency measured by an observer is Doppler shifted. The amount of the shift depends on the relative velocity component along the line connecting the molecule and the observer. The magnitude of the Doppler shift is given by:

$$\Delta\nu = \nu_0 \frac{v}{c}, \quad (1)$$



where  $\nu_0$  is the frequency emitted by the molecule in its rest frame of reference,  $v$  is the relative velocity, and  $c$  is the speed of light. In the atmosphere, there are a large number of molecules in random motion, emitting radiation. For such an ensemble of emitting molecules, the magnitude of the Doppler broadening is given by:

$$\Delta\nu = \frac{\nu_0}{c} \sqrt{\frac{2kT}{m}}, \quad (2)$$

where  $k$  is Boltzmann's constant,  $m$  is the molecular mass, and  $T$  is the temperature. Due to the large number of molecules in the atmosphere, statistically it seems likely that as many molecules are moving towards an observer as are moving away. Therefore, the effect of Doppler broadening is symmetric about the central wavelength of the transition.

These broadening mechanisms show the importance of developing instruments to study molecular spectra with high resolution. For example, from Equation (2) it is apparent that the amount of Doppler broadening in a spectral line depends on temperature. By measuring emission lines with high resolution, the temperature of the atmosphere could be extrapolated. This temperature determination could lead to an improved understanding of the molecular density profiles and chemistry of the atmosphere (Wallace, 1992).

### III. THEORY

In this section, an overview of the physical processes involved in the operation of the interferometer is given. The general nature of interference and coherence is discussed, followed by a description of diffraction from a single slit, multiple slits, and gratings. Finally the actual operation of the all-reflection Michelson interferometer is explained.

#### A. INTERFERENCE

The term interference is used to describe the interaction which occurs when light rays from a single source are recombined after having traversed different optical paths. This effect is a consequence of the wave nature of light.

A light wave consists of two transverse vector components propagating together, the electric field and the magnetic field. The propagation of a wave is generally described by specifying the evolution of the wave's electric field vector in time and space. The quantity which is actually measured by the eye and most other optical detectors, however is the irradiance. The irradiance is proportional to the time average of the electric field amplitude squared. For example, a plane wave with angular frequency  $\omega$  and propagation vector  $\bar{k}$  ( $k = 2\pi / \lambda$ ), observed at a position  $\bar{r}$ , is described by the equation:

$$\bar{E} = \bar{E}_0 e^{i(\bar{k} \cdot \bar{r} - \omega t)}, \quad (3)$$

and has an irradiance given by:

$$I = \epsilon_0 c \langle \bar{E} \cdot \bar{E}^* \rangle, \quad (4)$$

where the angled brackets represent the time average of the quantity inside. The quantity  $(\vec{k} \cdot \vec{r} - \omega t)$  is known as the phase of the wave. Surfaces of constant phase are called wavefronts.

Consider two waves with the same amplitude propagating in the same direction, which is assumed to be parallel to  $\vec{r}$ . Assume that their polarization is the same so that we need only consider the amplitude of the electric field and not its direction in comparing the two waves. The waves are described by:

$$E_1 = E_0 e^{i(kr - \omega t)}, \quad (5)$$

and

$$E_2 = E_0 e^{i(kr - \omega t + \phi)}, \quad (6)$$

where  $k$  is the wave number,  $\omega$  the angular frequency, and  $\phi$  the phase difference between the two waves. Each wave individually has the same irradiance, given by:

$$I_0 = \frac{1}{2} \epsilon_0 c E_0^2 \quad (7)$$

The total field at the point  $\vec{r}$  is:

$$\begin{aligned} E &= E_1 + E_2 \\ &= E_0 e^{i(kr - \omega t)} (1 + e^{i\phi}) \\ &= E_0 e^{i(kr - \omega t + \frac{\phi}{2})} \left( e^{-i\frac{\phi}{2}} + e^{i\frac{\phi}{2}} \right) \end{aligned}$$

$$\text{or} \quad E = E_0 e^{i(kr - \omega t + \phi/2)} [2 \cos(\phi/2)], \quad (8)$$

so that the irradiance is:

$$I = 2 \epsilon_0 c E_0^2 \cos^2(\phi/2), \quad (9)$$

$$\text{or} \quad I = 4 I_0 \cos^2\left(\frac{\phi}{2}\right). \quad (10)$$

Interference can be produced from splitting a wavefront into two parts, allowing each part to travel through a different path, and then recombining the two beams. An

example of this effect is double-slit interference, first demonstrated by Young in 1802. Monochromatic, collimated light is allowed to strike an opaque screen which contains two small slits a short distance apart, and the resulting pattern is viewed on a second screen a long distance away. This situation is depicted in Figure 4. In this figure,  $y$  is the distance between the slits,  $x$  is the distance from the slits to the viewing screen,  $\theta$  is the angle between the axis of the system and the observation point, and  $d$  is the difference between the two optical paths.

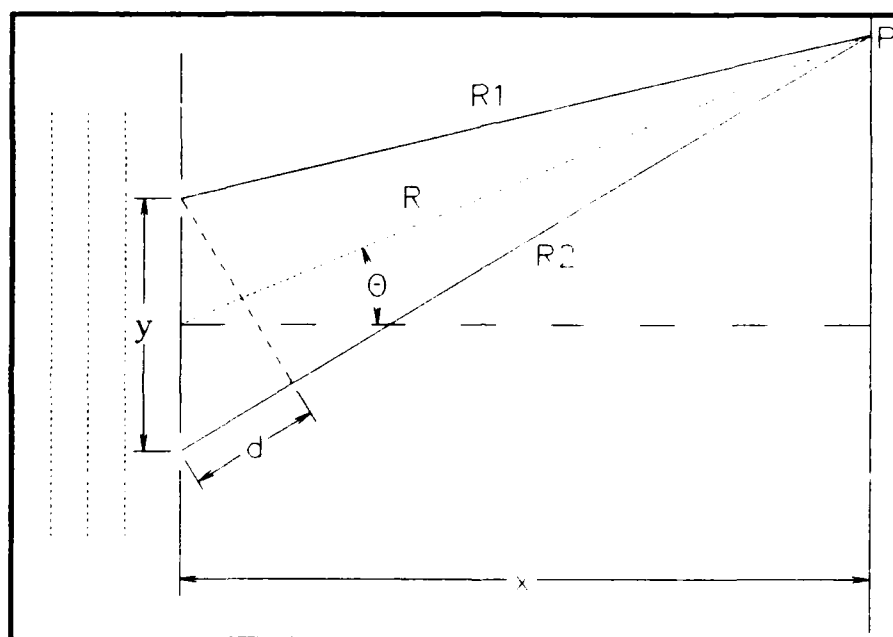


Figure 4 Double-Slit Interference

Since the illumination is assumed to be monochromatic, the propagation vector for the wave leaving each slit has the same magnitude,  $2\pi/\lambda$ . Polarization is not important here, so we will consider only the amplitudes of the two waves, which are both  $E_0$ . The electric field at the observation point  $P$  is the superposition of the fields coming from each slit at that point, so the irradiance is given by Equation (10). To find the phase difference

between the two waves, we make the approximation that the distance from the slits to the observing screen is large compared to the slit separation. This allows the approximation of the optical path difference  $d \approx y \sin \theta$ , so that the waves have a phase difference given by:

$$\phi = \left( \frac{2\pi}{\lambda} \right) y \sin \theta. \quad (11)$$

Substitution into Equation (10) produces an irradiance at the observing screen of:

$$I = 4I_0 \cos^2 \left( \frac{\pi y \sin \theta}{\lambda} \right). \quad (12)$$

From Equation (12), we can see that the irradiance on the screen is a maximum when the optical path difference is an integer multiple of  $\lambda$ , and a minimum when the difference is a half-integer multiple of  $\lambda$ . If we restrict ourselves to observing points on the viewing screen which are near the optical axis so that the off-axis distance  $Y \ll x$ , then we can make the approximation that  $\sin \theta \approx \tan \theta \approx \theta$ . Then:

$$I = 4I_0 \cos^2 \left( \frac{\pi y Y}{\lambda x} \right), \quad (13)$$

so that the screen will display equally spaced bright fringes separated by a distance of:

$$\Delta Y = \left( \frac{\lambda x}{y} \right). \quad (14)$$

In order for interference fringes to be visible in an interferometric device, the phase difference between the light from the different paths involved must be constant over the observation time. In the analysis above, the assumption was made that the incident light was a plane wave propagating as a perfect sinusoid. The production of light is an atomic process which occurs at many different points in the source, with no particular coordination between the many emitting atoms. Therefore, with most actual sources such as incandescent lamps and discharge tubes, the light is not emitted as an infinite sinusoid. Rather, it is emitted in quasi-sinusoidal packets called wavetrains. The wavetrains leaving

the source have a random distribution of initial phases. This tends to prevent the formation of interference fringes. These wavetrains have a characteristic length, known as the coherence length. Over this length the light can be considered to have a constant initial phase. In order for an interferometer to function, it must recombine light from corresponding wavetrains. This is achieved by making the input aperture approximate a point source of light, and by making the optical path difference smaller than the coherence length of the light source being used. Lasers produce light through a cooperative effort of many atoms in the active medium, and have an extremely long coherence length as a result. This makes it very easy to produce interference patterns with a laboratory laser. For a more detailed treatment of this subject, see Pedrotti and Pedrotti (1987).

## **B. DIFFRACTION**

Diffraction is a term used to describe the interaction of light waves with physical objects. The mathematical treatment of this phenomenon is generally considered in one of two approximations: Fresnel, or near-field diffraction, and Fraunhofer, or far-field diffraction. It is far-field diffraction that is of concern in this thesis, so only a discussion of Fraunhofer diffraction will be given here. A more complete treatment of this subject can be found in Pedrotti and Pedrotti (1987) or Taylor (1987).

Diffraction effects are a consequence of the Huygens-Fresnel principle, which says that every point on a wavefront acts as a source of secondary spherical wavelets, and that the field at any other point is the sum of these secondary wavelets added in both amplitude and phase. When a plane wavefront encounters a small aperture in an opaque screen, the part of the wavefront striking the center of the aperture continues to propagate in the same direction, while the part of the wavefront near the edges of the aperture is bent. Viewed from a great distance away, the new wavefront will appear to be spherical. The

combination of secondary wavelets results in an intensity distribution on the far side of the aperture which peaks along the aperture axis, and decreases as the observer moves away from the optical axis. The geometry of the aperture controls the shape of the intensity distribution.

When a second aperture is placed near the first, the interference effects described above are superimposed on the diffraction pattern from each of the apertures. What is seen on a viewing screen is a series of light and dark fringes, with the intensity of the bright fringes decreasing as the off-axis distance is increased.

A diffraction grating can be considered to be a large number of regularly spaced slits, all diffracting the incoming light into mutually interfering beams. The cumulative effect of the interference is to create a series of widely spaced directions in which constructive interference occurs. These are called diffraction orders. This is illustrated in Figure 5. The directions of the various diffraction orders are described by the grating equation:

$$m\lambda = a \sin \theta, \quad (15)$$

in which  $m$  is the diffraction order,  $\lambda$  is the wavelength of the light,  $a$  is the distance between adjacent slits, and  $\theta$  is the angle from the grating normal.

A reflection grating can also be developed, with alternating areas of reflection and non-reflection made by inscribing a series of grooves on a reflective material. With the grooves replacing the sequence of slits in a transmission grating and assuming normal incidence, the reflection grating is also described by Equation (15).

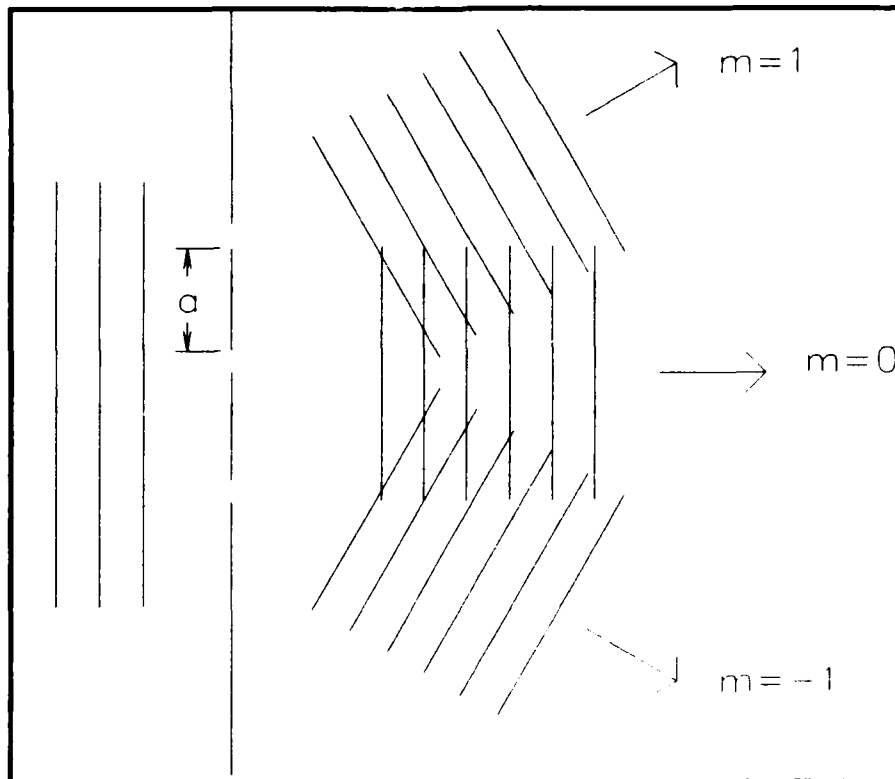


Figure 5 Diffraction Orders ( After Wallace, 1992)

If, however, the incident light is not normal to the grating, the equation describing the diffraction orders becomes:

$$m\lambda = a(\sin \theta_i + \sin \theta_m), \quad (16)$$

where  $\theta_i$  is the incidence angle, and  $\theta_m$  is the angle of the  $m$ 'th diffraction order, both measured clockwise from the grating normal. Diffraction from a plane grating with oblique incidence is depicted in Figure 6.



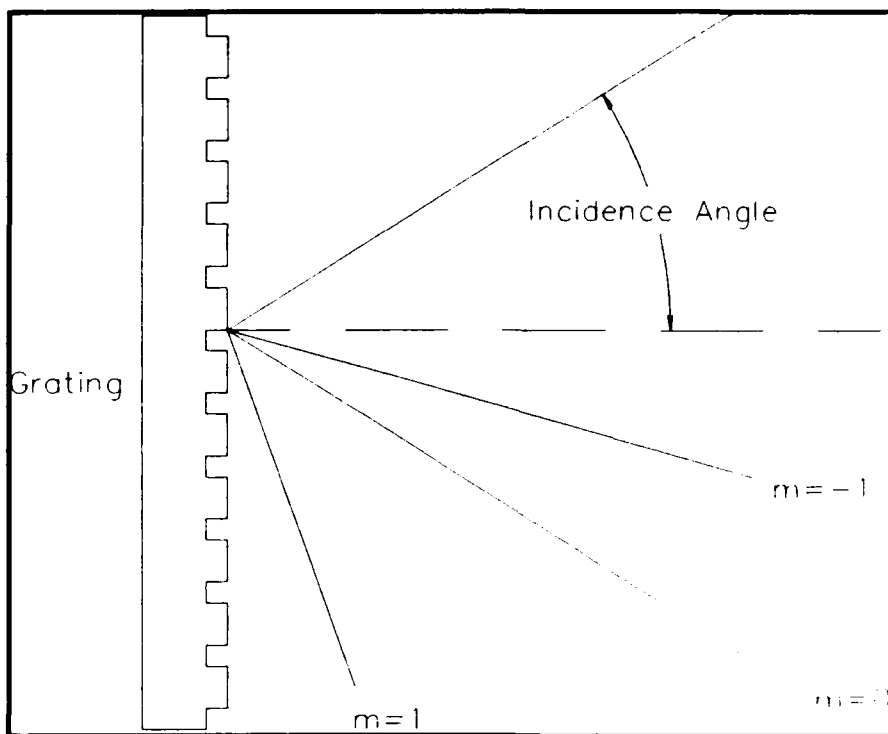


Figure 6 Diffraction With Oblique Incidence

### C. THE ALL-REFLECTION MICHELSON INTERFEROMETER

The instrument design being tested in this thesis is a Michelson interferometer modified to be constructed of only reflective optical elements. This is necessary as a result of a relative lack of suitable window materials in the wavelength range of the instrument's intended use, the ultraviolet. This device uses a plane diffraction grating and two plane mirrors to separate collimated light into two paths, then recombines the beams so that the interference pattern can be studied at the detector. The instrument produces linear interference fringes from which the input spectrum can be recovered by Fourier analysis.

The layout of a conventional Michelson interferometer is shown schematically in Figure 7. Collimated light strikes a partially silvered mirror positioned at a 45 degree angle to the incident beam. This splits the light into two beams which continue to propagate as plane waves but at right angles to one another. One beam is directed towards a fixed plane

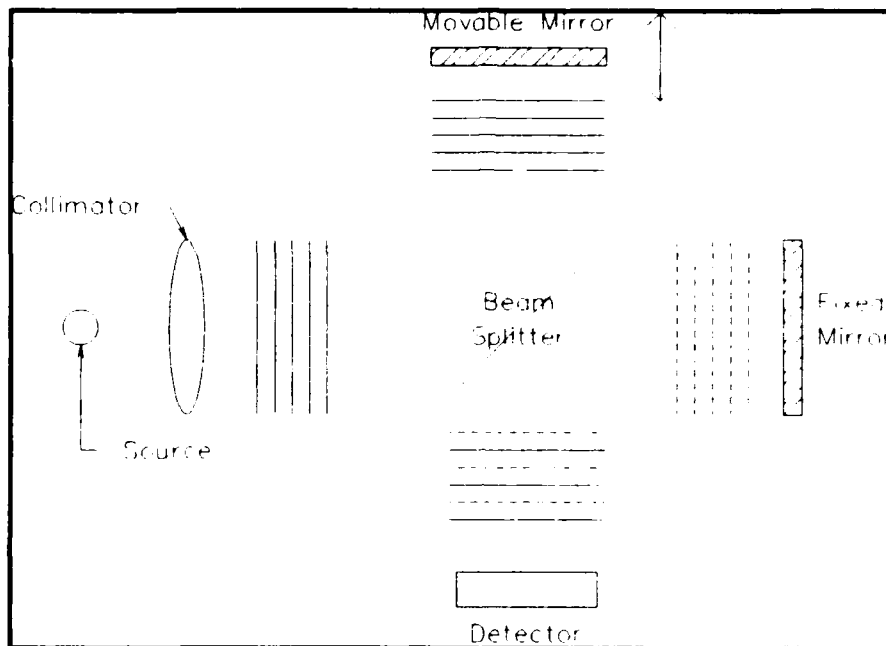
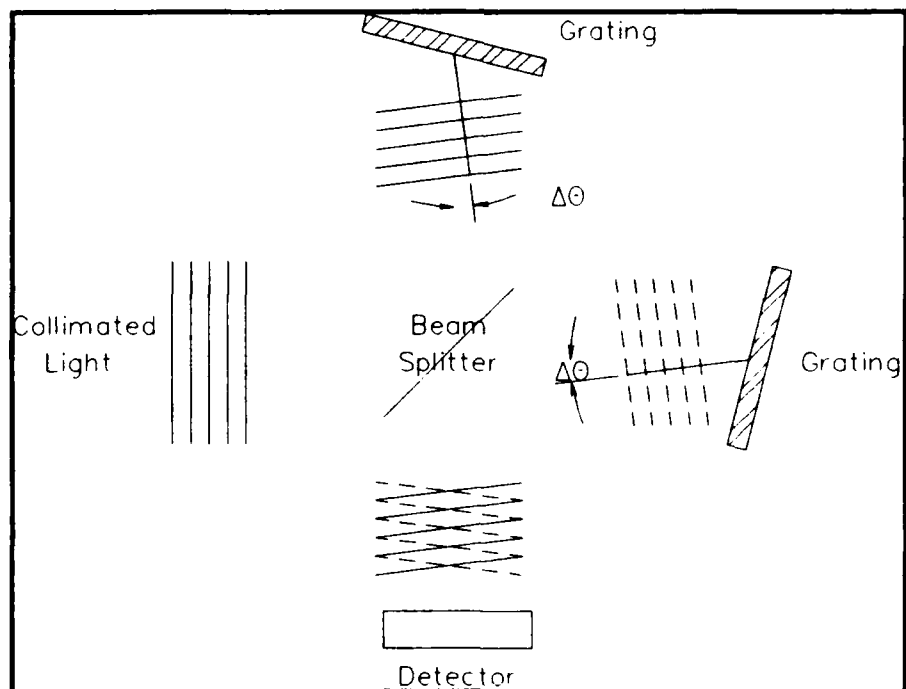


Figure 7 Michelson Interferometer

mirror while the other is directed towards a second plane mirror which can be translated along the line in which the light is propagating. The beams returning from the two mirrors are recombined at the beam splitter, and continue together towards the detector. Different detected irradiances can be produced by deliberately causing differences in the distances traveled by the two beams. If the path difference is zero, constructive interference results, and a bright spot is seen at the detector position. As the movable mirror is translated, the output at the detector alternates from bright constructive interference to dark destructive

interference. The output goes through one cycle as the movable mirror traverses a distance of one half the wavelength of the light being studied. In order to maximize contrast between light and dark fringes, it is important that the intensity of the two beams be the same.

Now consider a modification to the Michelson interferometer. Suppose the two plane mirrors were replaced by identical diffraction gratings, and positioned so that the distance from the beam splitter to each grating was the same. Further, assume that each grating was rotated through an angle  $\theta$  so that the incoming light struck each grating at an angle of incidence which was equal to the angle of one of the diffraction orders for the wavelength of light being studied. The effect of the grating rotation is to tune the interferometer for a particular wavelength,  $\lambda_0$ . If monochromatic light with wavelength  $\lambda_0$  is incident on this modified instrument, constructive interference will be seen at the detector. If, however, the light entering the interferometer has a different wavelength, such as  $\lambda_0 + \Delta\lambda$ , the wavefronts leaving the two gratings will make an angle  $\Delta\theta$  with the grating normals. This angle is proportional to the difference  $\Delta\lambda$  between the input wavelength and the tuned wavelength,  $\lambda_0$ . When the two beams recombine at the beam splitter, the angular separation between their wavefronts will cause a series of linear bright and dark fringes to appear at the detector. The spatial frequency of these fringes will depend on the angle  $\Delta\theta$  and ultimately on the wavelength difference  $\Delta\lambda$ . This situation is depicted in the diagrams Figure 8 and Figure 9.



**Figure 8**      **Modified Michelson Interferometer**

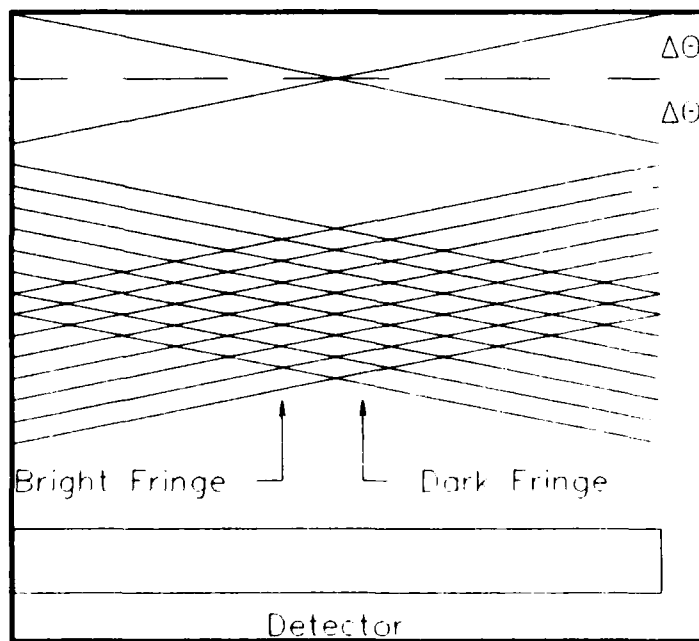


**Figure 9**      **Expanded View of Interference Fringes**

The prototype instrument being tested uses the modified Michelson interferometer design described above, with additional modifications to meet the requirement to construct the instrument from all-reflective optical elements. As depicted in Figure 10, a single plane diffraction grating serves as both the beam-splitting element and as the element which disperses the light by wavelength. This eliminates any problems with aligning multiple gratings, and prevents difficulties arising from differences in grating ruling density. The intensities of the two beams used are kept equivalent by having each beam undergo both a zero-order diffraction and a minus-one-order diffraction before being recombined, while

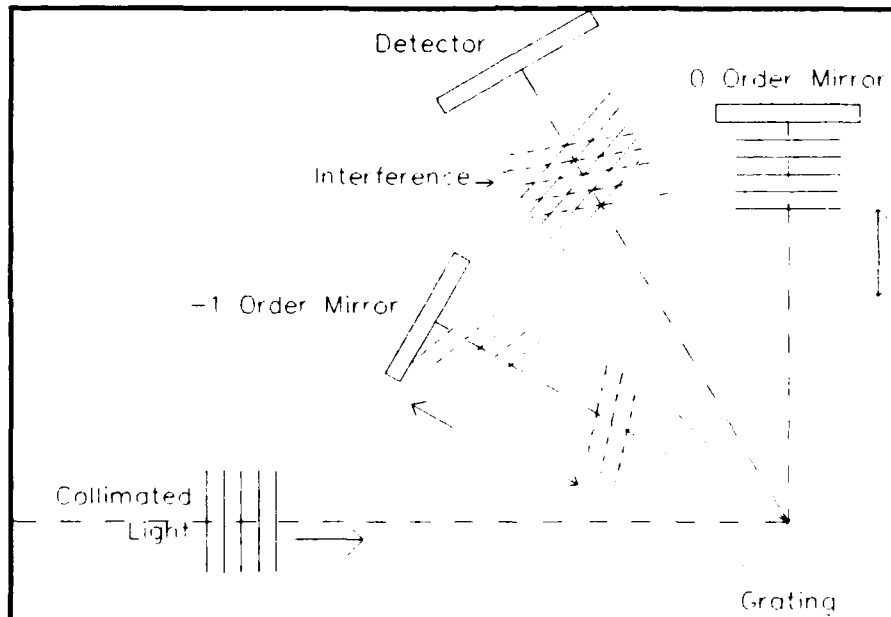


Figure 10 All-Reflective Michelson Interferometer

the path lengths for each beam are identical. An interference pattern, or interferogram, results from the angular separation between the beams caused by the difference in the incident wavelength from the tuned wavelength.

This design is lightweight, and can be made compact for inclusion in a rocket or satellite. It has been shown (Cleary et. al, 1992; Wallace, 1992) that the throughput of light can be optimized by using a grating ruling density which eliminates unused diffraction orders. Wallace (1992) calculated a resolution for the instrument of:

$$\Delta\lambda_{\min} = \frac{\lambda_0}{2L} \sqrt{a^2 - \left(\frac{\lambda_0}{2}\right)^2}, \quad (17)$$

where  $\lambda_0$  is the tuned wavelength,  $a$  is the space between grating lines, and  $L$  is the length of the sensitive region of the detector. For the oxygen emission at 1304 Å, using an optimized grating ruling density of 6000 lines/mm and detector length of one inch, the resolution is better than four milliångstroms. By enabling in-flight realignment, it would be possible to study more than one emission line during the same mission.

## **IV. EXPERIMENT**

In this section, the experimental procedures used in the construction and testing of the prototype all-reflective Michelson interferometer are discussed.

### **A. CONSTRUCTION OF ALL-REFLECTIVE INSTRUMENT**

The feasibility of the all-reflective Michelson interferometer was demonstrated by Wallace (1992). He built a prototype instrument that used visible light from a He-Ne laser as a source, with the light being collimated by an arrangement using a beam expander and a convex lens. The starting point for the current work was to replicate his results using the same light source and instrument geometry, but incorporating an off-axis parabolic mirror as the collimating device. This was an important step because a practical instrument for use in space will have to be constructed using only reflective optical elements.

While preparing to construct the prototype interferometer, the decision was made to mount the light source, aperture, and collimating mirror on an optical rail, which would then be secured to the laboratory bench. The reason for this was to make it possible to change the position and direction of the instrument's input beam without requiring a time-consuming alignment procedure, since all of the elements involved in the collimation process could be moved as a single unit.

To use an off-axis parabolic mirror as a collimator, it was necessary to make the incoming light approximate a point source located at the focus of the original paraboloid from which the off-axis mirror was sectioned. This was accomplished by mounting a circular pinhole 100  $\mu\text{m}$  in diameter in a modified optical fiber holder. This allowed the pinhole to be translated in a plane perpendicular to both the optical bench and the incoming laser beam, using small thumbscrews. The holder was attached to a carrier which

would move along the optical rail to adjust the distances from the pinhole to the light source and to the parabolic mirror.

An Oriel Model 45347 off-axis parabolic mirror was mounted so that its symmetry plane was at the same height above the bench as the input beam and the pinhole. It was situated on a pair of crossed translation stages which were attached to the optical rail. This allowed the mirror to be moved freely in a plane parallel to the optical bench using micrometer adjustments on the translation stages. The initial placement of the mirror relative to the pinhole was accomplished using a ruler and the published specifications of the mirror. The center of the mirror was placed along the input beam line at a distance of 11.9 cm from the pinhole.

Since collimated light can be considered the output of a point source located an infinite distance away, a telescope focused at infinity provides a focused image of the illuminated pinhole when the parabolic mirror is situated at the proper location to collimate the incoming light. Alignment of the mirror was first attempted using a Meade 10 inch reflecting telescope. The telescope was focused at infinity by observing the moon, and the position of the focus knob was noted. A microscope lamp was used to illuminate the pinhole, and the telescope was placed in position to look into the face of the mirror. The field-of-view of this large astronomical telescope was so small that locating the reflection of the pinhole was extremely difficult. Once the reflection was positioned within the viewing area, it was found that the magnifying power of the telescope was so large that only a small part of the pinhole image could be seen. As adjustments were made to the mirror position to improve the focus of the image, the image would move out of the telescope field of view, requiring the process of locating the reflected beam to begin again. Eventually, the decision was made to abandon this large reflecting telescope and to continue the alignment of the collimating mirror using a smaller telescope with less magnifying power.



A small refracting telescope was obtained and set for an effective distance of infinity by focusing on an object several miles away. The focusing mechanism was then locked in place using a metal band. This calibrated telescope was mounted on the optical bench and co-aligned with the parabolic mirror. A microscope lamp was again used to illuminate the pinhole, and micrometer adjustments on the translation stages were used to adjust the mirror position until the best possible image of the pinhole was obtained in the telescope eyepiece. This was a somewhat subjective judgment, because the best image was in fact a pair of images offset by approximately the radius of the pinhole. This was attributed to small aberrations visible on the surface of the parabolic mirror. The manufacturer's specification for the mirror indicated that the angle between the input beam and the outgoing collimated beam should have been 90 degrees, but this was not found to be the case. Rotating the mirror about an axis perpendicular to the optical table through an angle of about 10 degrees produced a sharp, circular image of the pinhole. At that point the light was considered to be collimated, and the controls were locked in place. The collimation was further verified by holding a viewing screen in the output beam and noticing that the beam diameter remained constant at several different distances from the collimating mirror.

A Class II He-Ne laser was mounted on the optical rail, and fitted with a Sharp 20X microscope objective as a beam expander. A convex lens with a focal length of 10 cm was used to focus the laser light onto the pinhole aperture. The use of this lens was for the sake of convenience only and was not an integral part of the instrument. In a practical model, incident light would be collected using a reflecting telescope and focused on the input pinhole or slit. The laser source used for this experiment combined with the pinhole and mirror arrangement provided an intense, coherent, collimated beam with a nearly monochromatic wavelength of 5435 Å.

A plane diffraction grating was mounted in a holder which allowed micrometer adjustment of its angles about axes both normal to and parallel to the plane of the optical bench. The grating was placed in such a way that the collimated beam struck its center at an incidence angle of approximately 28 degrees. Since the 1200 lines/mm ruling density of the grating was less than the optimal 1227 lines/mm for this wavelength (Wallace, 1992), there were unused diffraction orders produced. This was not a problem because of the high intensity of the source. The grating was adjusted to make its plane normal to the table by manipulating its tilt until all diffraction orders were intercepted at the same height above the optical bench as the input beam, 14.2 cm.

The secondary mirrors for the zero and minus-one orders were one inch diameter plane mirrors mounted in holders that allowed adjustment of their angles about two axes perpendicular to the mirror normals. These were positioned approximately 30 cm from the grating at positions that intercepted the zero and minus-one diffraction orders. The plane mirror rotation angles were adjusted so that the reflected beams struck the grating at the same point as the incident beam.

A CCD video camera with the lens removed was used as a detector. It was placed on the table so that the center of the detector area was illuminated by the recombined beams from the different diffraction orders. The camera was then connected to a black-and-white television monitor. With interference fringes visible on the screen, fine adjustments were made to the horizontal angle of the minus one order mirror to make the fringes vertical. A variation of input wavelength was simulated by rotating the minus one order mirror about an axis perpendicular to the optical bench. This was observed to change the spatial frequency of the fringes displayed, as expected. Figure 11 is a diagram showing the layout of the system.

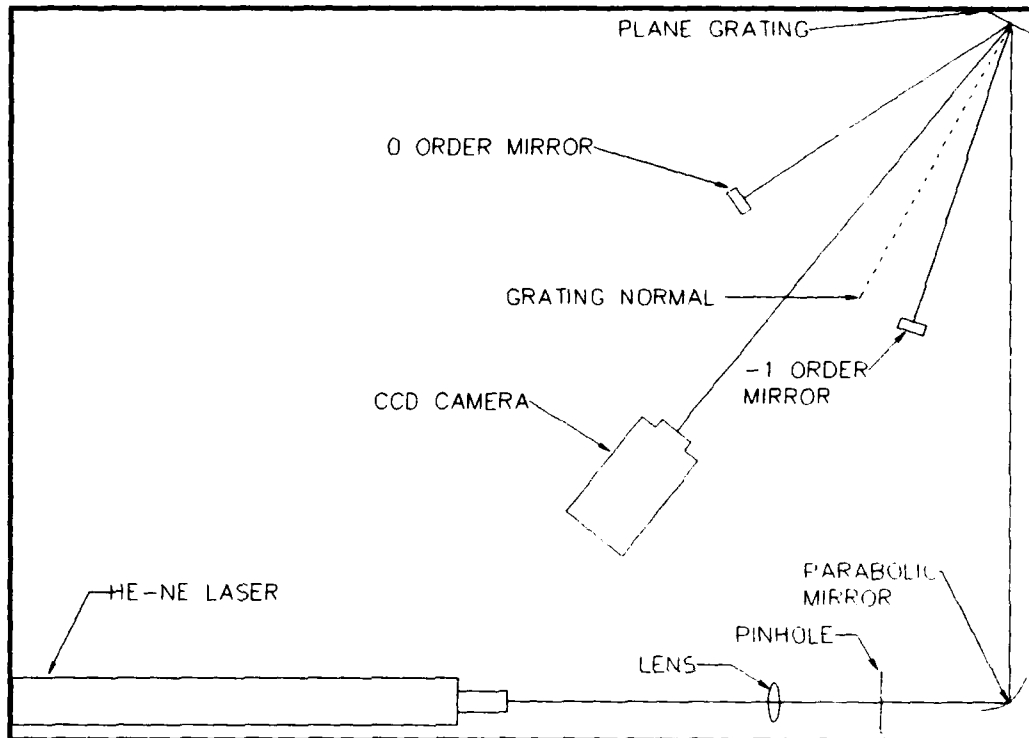


Figure 11 Interferometer Layout

## B. TESTING WITH SODIUM VAPOR LAMP SOURCE

The next step in testing the interferometer design was to assemble the prototype instrument using a light source with a coherence length shorter than that of the He-Ne laser. It was decided to study the sodium doublet emission at a wavelength of  $5889 \text{ \AA}$ . An Oriel Model 65160 lamp was fitted with a sodium vapor bulb, and mounted on the optical rail. The convex lens with a focal length of 10 cm was again used to focus the light onto the pinhole.

Alignment of the secondary mirrors was accomplished visually. The grating incidence angle was chosen to provide a convenient angular spread between the minus one order reflection and the detector angle. This allowed sufficient space for the detector and its associated wires to fit on the bench between the plane mirrors without blocking the

incident beam or any reflected beams. When all elements of the system were in place, it was noted that there were no interference fringes visible at the camera position, despite visual observation of the recombined beams entering the detector. This was attributed to there being too much loss of light from the system, between the unused diffraction orders from the grating and the four reflections involved in the instrument. Also, the performance of the camera was noticed to be erratic at low light levels, possibly due to a built-in gain control. Therefore, it was decided to test the system using a more intense light source.

### **C. TESTING WITH MERCURY VAPOR LAMP SOURCE**

Testing the interferometer using a mercury vapor source required the same general set-up as the sodium source. A low-pressure mercury discharge tube was placed in the Oriel lamp and mounted on the optical rail. A band-pass filter was installed to select the green line at a wavelength of 5461 Å. The proximity of this wavelength to the 5435 Å line of the He-Ne laser allowed a nearly identical instrument geometry to be used. The grating incidence angle was set to approximately 30 degrees.

As when setting up the instrument for the laser source, the alignment of the zero and minus-one-order mirrors was accomplished by observing the different diffraction orders from the grating, placing the mirrors visually in the beams, and then aligning them so that their return beams intercepted the grating at the same spot as the collimated incident light. The CCD camera was placed in the center of the recombined beams, but no interference fringes were visible on the television monitor. The camera was detecting some output light from the instrument, although the intensity was faint. Covering either of the secondary mirrors with an opaque card would result in a noticeable change in the brightness of the screen display. It was thought that an automatic gain correction in the camera might be preventing the display of the closely spaced bright and dark fringes which were expected

in the interference pattern, and that this problem could be overcome by finding some way of increasing the amount of light reaching the detector.

To increase the throughput of light in the instrument, the decision was made to enlarge the aperture at the start of the optical system. Replacing the 100  $\mu\text{m}$  pinhole with a circular aperture 250  $\mu\text{m}$  in diameter would allow approximately six times as much light to enter the system. It was felt that this change would not seriously degrade the degree of collimation in the input beam. The replacement of the pinhole made it necessary to re-align the off-axis parabolic mirror. This was accomplished using the small retracting telescope as was described above.

With the input aperture replaced and the collimating mirror aligned, only minor adjustments to the alignment of the secondary mirrors were needed to make the instrument ready for testing. When the camera was placed in position, interference fringes were observed on the television monitor. The spatial frequency of the interference pattern could be modified by making minute changes to the vertical angle of the minus one order mirror. This was the first time that the design for the all-reflective interferometer was shown to work using a source whose coherence length was shorter than that of a laboratory laser. The next step was to obtain a quantitative measure of the intensity distribution in the interference pattern by using a linear photodiode array for the detector. Before we could accomplish this, unfortunately, the prototype stopped working. We could no longer reproduce the interference fringes on the CCD camera. It was suspected that one of the micrometer adjustments affecting the instrument alignment had been inadvertently moved, but attempts to regain the interference pattern by re-adjusting the alignment proved fruitless.

In an effort to trace the cause of the failure, a conventional Michelson interferometer was used to measure the coherence length of the mercury discharge lamp being used as the light source for the experiment. This length was found to vary from approximately 2.5

mm when the lamp was first turned on, decreasing to a stabilized value of about 2.0 mm after the vapor pressure of mercury in the tube had built up through 10 minutes of operation. In order for a stable interference pattern to be formed, the difference in the lengths of the paths between the grating and the two secondary mirrors had to be less than 2.0 mm. Out of a desire to avoid damage to the plane mirrors or the diffraction grating, the instrument had been assembled without allowing a measuring device to touch any of the surfaces, so it was doubtful that this tolerance in optical path matching had been obtained. This problem provided a possible explanation for the intermittent performance of the prototype. Evidently, the path length difference had been within the coherence length of the source at first, allowing an interference pattern to be seen. When the controls were accidentally moved, the mismatch in path lengths exceeded the 2.0 mm coherence length, and the fringes disappeared. During subsequent attempts to re-align the instrument, a functional configuration was never attained.

While positioning the plane mirrors to within a path length difference of several millimeters without touching any sensitive surfaces with a ruler seemed difficult, they could easily be placed to an accuracy within a centimeter. It seemed that a mercury discharge lamp with a longer coherence length might make the instrument work. Discharge lamps used in lecture demonstrations were known to have relatively long coherence lengths. A mercury "pen-ray" was obtained, and the band-pass filter described above was used to select the green 5461 Å emission. The coherence length of this emission was measured using the conventional Michelson interferometer, and found to be approximately 2.5 cm. The pen-ray was mounted as the light source in the prototype instrument. The two secondary mirrors were positioned as accurately as possible and aligned as described above. Unfortunately, the new source was not bright enough to provide detectable levels of light at the camera position, a result of the low transmittance of the filter at 5461 Å. As a result, testing using the mercury green line was abandoned.

#### **D. TESTING WITH ULTRAVIOLET SOURCE**

In order to obtain successful results from the prototype instrument, a more intense source was needed. Accordingly, the decision was made to move directly to a source in the ultraviolet wavelength range. After standard tables were consulted (Corliss, 1962, Reader and Corliss, 1980), the mercury line at a wavelength of 2537 Å was chosen for study. This emission was approximately 15 times as intense as the green line used above, and could be expected to have a longer coherence length.

The ultimate goal of the testing being conducted was to verify the feasibility of the interferometer design for studying ultraviolet emissions. It had become clear that assembling the prototype instrument to distance tolerances tight enough to allow the device to work would be very difficult. Moving to the 2537 Å emission would allow the goal to be reached without having to carefully construct several more prototype instruments.

In designing the layout for the ultraviolet experiment, the first step was to choose the grating incidence angle. An angle of 45 degrees was chosen so that the incident beam would be perpendicular to the zero order diffraction. It was thought that this would make it easier to set the grating to the proper incidence angle using a carpenter's square and a visible laser. This was later found to be unnecessary when the alignment method described below was developed.

Computer simulation of the all-reflective Michelson interferometer has shown that deviation in the incident light from collimation would severely degrade the interference pattern observed (Carlson, 1993). To minimize this effect, a short distance between the grating and the plane mirrors was desired. Taking the size of the equipment needed to mount the plane mirrors and detector into consideration, a distance of 20 cm was chosen.

Moving the wavelength of the experiment into the ultraviolet range presented a new set of problems for assembling the prototype, the most important one being that ultraviolet

light is not visible to the human eye. This meant that the visual method of placing the plane mirrors in the correct positions which had been used previously would no longer be feasible. To get around this difficulty, the proper positions of the optical elements were calculated based on the design parameters chosen above. Then, a full-scale drawing of the instrument was produced using Autosketch, a two-dimensional drafting program for personal computers. This template showed the positions of the incident beam, the diffraction grating, the two plane mirrors, and the output beam to the detector. In addition, the position of the minus one order diffraction of a beam from the He-Ne laser is shown. Its use will be described below. Figure 12 is an example of the template used, although it is reproduced here at less than full scale.

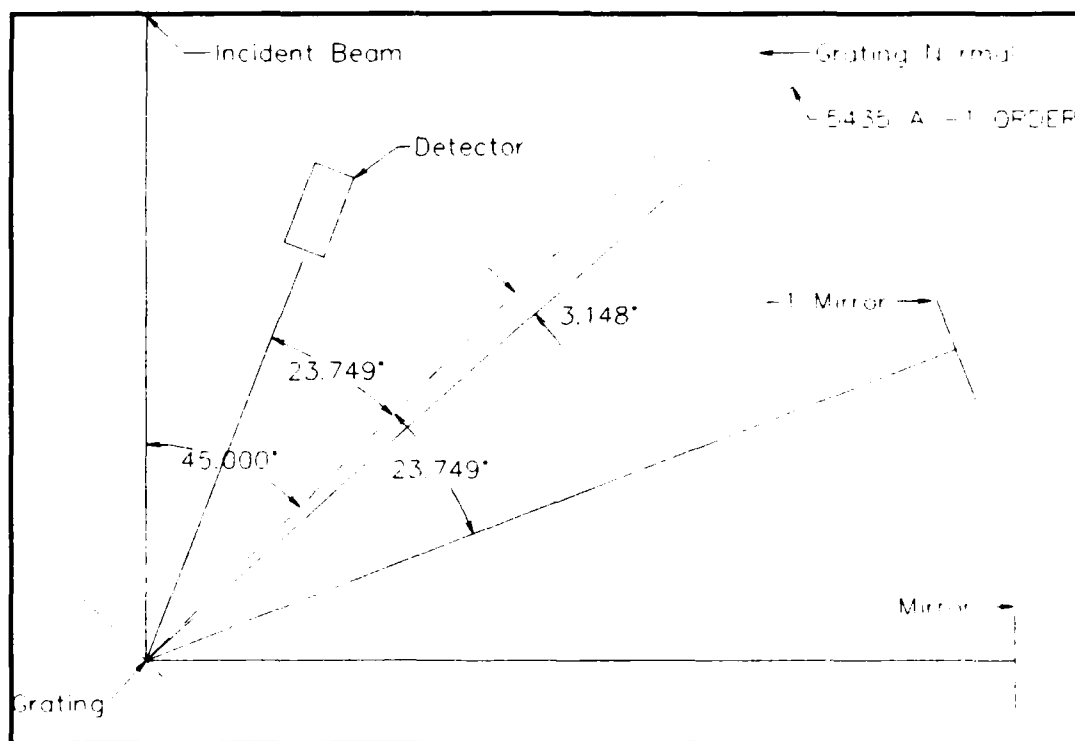


Figure 12 Ultraviolet Instrument Template



To position the template on the optical bench, a beam from the He-Ne laser with the beam expander removed was directed through the pinhole into the collimating mirror. A straight edge with an accurate right angle was used to trace out the path of the beam from the parabolic mirror to the diffraction grating. The position on the table was located by finding the intersection of the straight edge with the collimated laser beam, and marking the point on the table directly beneath the beam. The template was positioned with its input beam over the laser trace. The intersection point between the beam and the grating on the template was placed directly under the spot where the laser beam hit the grating. The template was then secured to the table, and the grating rotated until the zero order and minus one order diffracted beams left the grating exactly above the beams marked on the template. In this way, the desired incidence angle of 45 degrees was set. Next, the plane mirrors were positioned directly over their representations on the instrument template and secured to the table.

The zero order mirror remained in the same position regardless of wavelength, so the reflected laser beam struck it squarely in the center. The mirror was then aligned by adjusting its rotational controls so that the return beam hit the diffraction grating at the same spot as the incident beam. Since the laser being used for alignment was operating at a visible wavelength, and the minus one order mirror had been positioned for 2537 Å light, there was no laser light striking this mirror. In order to align the minus one order mirror, a second laser was needed. The path of light from the minus one order mirror to the grating and on to the detector in the system is a zero order diffraction, which is independent of wavelength. So, a Class II He-Ne laser operating at 6328 Å was placed over the template, positioned at the point where the detector would eventually go, and aimed so that its spot hit the same point on the grating as the spot from the original laser. The zero order diffraction from this beam hit the minus one mirror. Rotational controls were used to

adjust the return beam to the same spot on the grating as the incident beam and return beam from the zero order mirror.

The next problem to be addressed was the detector. Since the wavelength being planned for this experiment was in the ultraviolet range, the camera used in the experiments described above was not suitable. An idea was developed to place a thin, uniform layer of some fluorescent material on a microscope slide, and then to place the slide in front of a linear photodiode array of the type used in the NPS MUSTANG instrument. It was known that the glowing powder would not provide a great deal of spatial resolution, but it was thought that it would suffice to qualitatively verify the presence of visible interference fringes.

The first detector material tried was the orange dye fluorescein. This powder dissolved readily in water, forming a solution that gave off a bright green-yellow glow when exposed to ultraviolet light. An attempt was made to create a thin layer of this material on a microscope slide by coating the slide with the fluorescein solution and allowing the solvent to evaporate away, but it turned out that the powder that precipitated onto the plate no longer glowed. Evidently, the fluorescent properties were associated only with the fluorescein ions in solution. There was no convenient way to expose a liquid solution to the ultraviolet light in the prototype instrument, so another detector material had to be located.

Another available powder known to fluoresce in ultraviolet light was 1,4-diphenylbenzene, called "spy dust". A saturated solution was prepared by gradually mixing the powder into 10 ml of benzene until no additional crystals would dissolve. This solution was coated onto microscope slides, which were kept in a fume hood until the solvent evaporated away. This left a fine coating of the pale violet powder on the slides, which gave off a noticeable glow in the presence of ultraviolet light. It was found, however, that the slides did not glow brightly enough to be of use when placed in the detector position

of the bench-top instrument because the intensity of the light reaching that point was too low. Nevertheless, the powder detectors were used to verify the alignment of the instrument by placing the pen-ray source on the input beam position in front of the diffraction grating, and observing the glow localized at the zero and minus one order plane mirrors.

It was decided to build a detector assembly using an ITT model F4145 microchannel plate image intensifier, and Hamamatsu S3904-1024F linear photodiode array. Photons entering the image intensifier strike a photocathode, causing electrons to be ejected. These electrons are accelerated by an electrical potential within the device, and enter the microchannel plate, where amplification occurs while preserving the electrons' spatial resolution. The large number of electrons produced is accelerated through the plate. The electrons strike a phosphor screen, which emits visible light. The linear photodiode array is situated behind the phosphor screen, and each of its 1024 pixels produces an analog signal proportional to the intensity of the light striking the photodiode. These signals are read using a Labview program developed for the purpose on the Macintosh computer.

The detector assembly was first placed on the optical table so that it would be exposed to the collimated beam leaving the off-axis parabolic mirror. The pen-ray lamp was turned on, and a strong signal was observed on the computer readout of the linear detector array. A narrow slit was then placed in front of the image intensifier tube and moved from side to side while the detector readout was observed. A peak corresponding to the slit was seen to move back and forth on the computer display. This verified the operation of the detector assembly.

Next, the detector assembly was placed in its proper position in the instrument layout. For alignment purposes, a narrow slit was placed in the collimated beam between the off-axis parabolic mirror and the diffraction grating. The zero-order mirror was covered with an opaque cloth so that only the beam reflected from the minus-one-order

mirror could be observed at the detector. The computer display showed a well-defined peak corresponding to the output beam. This peak was observed to move from side to side on the display when the angle of the minus-one-order mirror was rotated about the vertical axis of the optical table. The mirror was rotated to bring the peak to the center of the detector array.

The minus-one-order mirror was then covered in order to observe the alignment of the zero-order mirror. Unfortunately, no return beam was visible on the computer display. The image intensifier gain was increased by approximately a factor of four, and still no return beam was visible. The zero-order mirror was rotated about the vertical axis through an angle of several degrees on either side of its previously set position, but no change in the detector signal was observed. The reason for this problem is not fully understood. It is thought that the blaze angle of the diffraction grating may be preventing enough light from being diffracted into the minus-one-order towards the detector when the return beam from the zero-order mirror strikes the grating.

## **V. RESULTS AND RECOMMENDATIONS**

### **A. RESULTS OF EXPERIMENTS**

During the experiments conducted for this study, the design for an all-reflection Michelson interferometer was tested using several different light sources. The use of an off-axis parabolic mirror for collimation was shown to be feasible by the successful production of interference patterns using a laser light source.

While interference patterns were not reliably produced using the shorter coherence length visible light sources, the instrument was observed to work properly for a time using the visible green line of a mercury vapor lamp. The difficulties encountered were not the results of defects in the design of the interferometer. Rather, they arose out of the *limitations imposed on the construction of the prototype instrument on the optical bench.* Specifically, these limitations were: 1) The difficulty of making the path lengths between the diffraction grating and the secondary mirrors agree to within the coherence length of the light source prevented *stable interference fringes from appearing.* 2) Low sensitivity of the CCD camera may have obscured patterns which might have been observable with another detector. 3) The off-axis parabolic mirror was of low quality and not the ideal choice for this application. 4) Problems associated with the use of a blazed diffraction grating.

Nevertheless, some useful information was gained from the study. The method of using a full-scale template to affect rough positioning of the optical elements was developed, the sensitivity of the device to path length differences was discovered, and the

efficacy of the image intensifier/linear photodiode array combination for use as an ultraviolet detector in this instrument was verified.

## **B. RECOMMENDATIONS FOR FURTHER STUDY**

The goal of developing an all-reflection instrument for use in space can best be attacked from this point by working in two directions simultaneously. First, a means of developing a functional prototype instrument on the bench-top must be pursued. This can be accomplished by obtaining mirror mounts which can be positioned with a greater degree of accuracy, locating intense, coherent visible light sources, and obtaining a better video camera for use as a visible light detector. Once a reliable prototype has been produced, the sensitivity of the instrument to fluctuations in temperature and vibration should be investigated.

Secondly, engineering development for a flight instrument should be begun, ensuring close tolerances for the mirror path lengths and tight specifications for the off-axis parabolic mirror and diffraction grating. Moreover, it would appear that a non-blazed grating would be more suitable for this application. With these tasks accomplished, there is no doubt that the all-reflection Michelson interferometer will provide valuable information about the atmosphere in the future.

## LIST OF REFERENCES

Atkinson, J. D., IV, *Implementation and Use of a Computational Ray-Tracing Program for the Design and Analysis of Complex Optical Systems*, Master's Thesis, Naval Postgraduate School, Monterey, California, March 1993.

Carlson, Scott. M., *Validation of the Design of a High Resolution All-Reflection Michelson Interferometer For Atmospheric Spectroscopy*, Master's Thesis, Naval Postgraduate School, Monterey, California, June 1993.

Chase, B. E., *A Calibration of the Naval Postgraduate School Middle Ultraviolet Spectrograph (MUSTANG)*, Master's Thesis, Naval Postgraduate School, Monterey, California, September 1992.

Clayton, Michael J., *Analysis of the Ultraviolet Emissions of Nitric Oxide From Mid-Latitude Rocket Observations*, Master's Thesis, Naval Postgraduate School, Monterey, California, June 1990.

Cleary, D. D., Nichols, J., and Davis, D. S., "Design for an All-Reflection Michelson Interferometer", *Applied Optics*, 31, 433, 1992.

Corliss, Charles H., and Bozman, William R., *Experimental Transition Probabilities for Spectral Lines of Seventy Elements*, National Bureau of Standards Monograph 53, United States Department of Commerce, 1962.

Dirac, P. A. M., *The Principles of Quantum Mechanics, Fourth Edition*, Oxford University Press, Oxford, England, 1958.

Eisberg, Robert, and Resnick, Robert, *Quantum Physics of Atoms, Molecules, Solids, Nuclei, and Particles, Second Edition*, John Wiley and Sons, New York, 1985.

Nichols, J., *The Design of a New Far Ultraviolet Interferometer for Ionospheric Spectroscopy*, Master's Thesis, Naval Postgraduate School, Monterey, California, December 1990.

Pedrotti, F. L., and Pedrotti, L. S., *Introduction to Optics*, Prentice-Hall, Inc., Englewood Cliffs, New Jersey, 1987.

Reader, Joseph, and Corliss, Charles H., *Wavelengths and Transition Probabilities for Atoms and Atomic Ions, Part 1*, National Bureau of Standards Reference Data System 68, United States Department of Commerce, 1980.

Tascione, T. F., *Introduction to the Space Environment*, Orbit Book Company, Malabar, Florida, 1988.

Taylor, C., *Diffraction*, Adam Hilger, Bristol, England, 1987.

Walden, Billie S., *An Analysis of Middle Ultraviolet Dayglow Spectra*, Master's Thesis, Naval Postgraduate School, Monterey, California, December 1991.

Wallace, Kenneth M., *Design of a High Resolution Spatial Heterodyne Interferometer*, Master's Thesis, Naval Postgraduate School, Monterey, California, December 1992.



### INITIAL DISTRIBUTION LIST

- |    |  |   |
|----|--|---|
| 1. | Defense Technical Information Center<br>Cameron Station<br>Alexandria, Virginia 22304-6145                           | 2 |
| 2. | Library, Code 52<br>Naval Postgraduate School<br>Monterey, California 93943-5002                                     | 2 |
| 3. | Dr. K. W. Woehler, Chairman PH<br>Physics Department<br>Naval Postgraduate School<br>Monterey, California 93943-5000 | 1 |
| 4. | Dr. D. D. Cleary, Code PH/CI<br>Physics Department<br>Naval Postgraduate School<br>Monterey, California 93943-5000   | 3 |
| 5. | Dr. D. S. Davis, Code PH/Dv<br>Physics Department<br>Naval Postgraduate School<br>Monterey, California 93943-5000    | 1 |
| 6. | Dr. Larry Paxton<br>Mail Stop 24-E115<br>Applied Physics Laboratory<br>Johns Hopkins Road<br>Laurel, Maryland 20723  | 1 |
| 7. | LT Allan David Risley, Jr.<br>901 Old Dominion Lane<br>Virginia Beach, Virginia 23451                                | 1 |